Rabi resonances induced by an off-resonant, stochastic field

J. C. Camparo, J. G. Coffer, and R. P. Frueholz
Mail Stop M2-253, Electronics Technology Center, The Aerospace Corporation, P.O. Box 92957, Los Angeles, California 90009
(Received 26 March 1998)

When an atom interacts with a phase-fluctuating field of fairly arbitrary spectral character, the Fourier spectrum of atomic population variations manifests a ''bright line'' at the atomic system's Rabi frequency. This bright line is termed a Rabi resonance. Here, we generalize our previous studies of this phenomenon by considering the characteristics of the Rabi resonance when it is excited by an *off-resonant* stochastic field. We find both experimentally and theoretically that (i) the Rabi resonance occurs at the Rabi *nutational* frequency, $\Omega=\sqrt{\Delta^2+\omega_1^2}$, where Δ is the detuning and ω_1 is the Rabi frequency, (ii) that the strength of the Rabi resonance is maximized when $|\Delta|$ equals ω_1, and (iii) that the strength of the Rabi resonance is an asymmetric function of detuning. [S1050-2947(98)03611-7]

PACS number(s): 42.50.Md, 42.50.Ar, 32.80.$-$t

I. INTRODUCTION

In previous work we investigated the response of an atom, in terms of its Bloch-vector components, to a phase-fluctuating field (PDF) [1] that was on resonance with an atomic transition [2,3]. In those studies we found that an atom's temporal response to a resonant PDF is essentially composed of just two components. On time scales long compared to a Rabi period, an adiabatic component manifests itself in the instantaneous frame of field-atom interactions as a figure-eight pattern of the Bloch-vector trajectory [4]. Additionally, there is a nonadiabatic component in the atom's temporal response that manifests itself as enhanced atomic population variations oscillating at the Rabi frequency, ω_1, similar to the oscillations of a damped, driven harmonic oscillator with its resonant frequency at ω_1. These oscillations are a reflection of what has come to be called the ''Rabi resonance'' of an atom. While the adiabatic figure-eight component is only readily apparent in the instantaneous frame, the nonadiabatic component is principally associated with atomic population variations, and therefore is unchanged by the choice of reference frame (i.e., instantaneous, rotating, or laboratory frame). Consequently, the Rabi resonance is easily accessible to experimental investigation, and has relevance to quantum electronic devices such as atomic clocks, whose operation depends on atomic population variations.

Rabi-resonance phenomena can be observed experimentally in several ways. Cappeller and Mueller [5] first noted the existence of Rabi resonances in experiments with a ^{199}Hg spin system, where the modulation frequency of a phase-modulated, resonant field was tuned through the Rabi-resonance condition. In their experiments, the Rabi resonance was manifested as a resonant enhancement in the amplitude of population oscillations occurring at twice the phase-modulation frequency. Our work manifests a Rabi-resonance phenomenon in a very different fashion. An atomic system interacts with a *broadband field*, and as a consequence the atom exhibits population fluctuations characterized by a broadband of Fourier frequencies. A Rabi resonance in our experiments is observed as a resonant enhancement of Fourier components whose frequencies are near the Rabi frequency. Though at a fundamental level these two Rabi-resonance phenomena may be intimately connected, representing the same intrinsic property of the atomic system, at the present time their exact relationship is unclear.

In the work to be discussed below, we generalize our previous results on stochastic-field induced Rabi resonances by considering the temporal response of an atom to *off-resonant* stochastic fields. Examining the Fourier spectrum of the atomic population variations we find that the Rabi resonance occurs at the Rabi nutational frequency, $\Omega=\sqrt{\Delta^2+\omega_1^2}$, where Δ is the field-atom detuning. This result is consistent with the findings of Anderson *et al.* [6] regarding fluorescence intensity fluctuations in a PDF, though our studies investigate the Rabi-resonance condition in much greater detail. Additionally, we have examined the strength of the Rabi resonance as a function of detuning. As will be shown below, the strength of the Rabi resonance is maximized for $|\Delta|=\omega_1$, and it is an asymmetric function of detuning. In the following section, the theory of stochastic-field induced Rabi resonances is generalized to off-resonant excitation, and then in Secs. III and IV an experiment is described verifying certain key elements of the theory's predictions.

II. THEORY

As the starting point for our analysis, we employ the two-level atom Bloch equations in the rotating frame. The equations are the same as those used previously [2], except now the field detuning Δ is included (i.e., $\Delta\equiv\omega_{\text{field}}-\omega_{\text{atom}}$),

$$\frac{dX}{dt}=-\gamma X+\Delta Y-\omega_1 Z\cos(\theta), \tag{1a}$$

$$\frac{dY}{dt}=-\gamma Y-\Delta X-\omega_1 Z\sin(\theta), \tag{1b}$$

$$\frac{dZ}{dt}=-\gamma(Z-Z_0)+\omega_1 Y\sin(\theta)+\omega_1 X\cos(\theta). \tag{1c}$$

In these expressions, the transverse and longitudinal relaxation rates have been equalized (i.e., $\gamma_1 = \gamma_2 = \gamma$, as would be appropriate in magnetic resonance experiments); Z is the value of the population imbalance between the two states (with Z_0 its value in the absence of the electromagnetic field), while X and Y correspond to the imaginary and real parts of the atomic coherence, respectively, and θ is the field's instantaneous phase in the rotating frame. We are particularly interested in the behavior of Z for comparison with the experimental results, and while the analysis is best performed in the instantaneous frame, the transformation from the rotating to the instantaneous frame has no effect on Z. Applying the following transformation equations to the appropriate Bloch vector components,

$$X_{\text{inst}} = \cos(\theta) X_{\text{rot}} + \sin(\theta) Y_{\text{rot}}, \tag{2a}$$

$$Y_{\text{inst}} = -\sin(\theta) X_{\text{rot}} + \cos(\theta) Y_{\text{rot}}, \tag{2b}$$

results in the three instantaneous frame Bloch-vector equations:

$$\frac{dX}{dt} = -\gamma X + \left(\frac{d\theta}{dt} + \Delta \right) Y - \omega_1 Z, \tag{3a}$$

$$\frac{dY}{dt} = -\gamma Y - \left(\frac{d\theta}{dt} + \Delta \right) X, \tag{3b}$$

$$\frac{dZ}{dt} = -\gamma (Z - Z_0) + \omega_1 X. \tag{3c}$$

(For ease of notation we have dropped the instantaneous frame subscript, it being understood in all the following expressions.) Note that the principal simplification of the Bloch equations in the instantaneous frame is that the field's phase variation now appears directly as a multiplicative factor rather than the argument of a transcendental function [7].

As in our previous work, the phase variations are written as the sum of adiabatic and nonadiabatic components:

$$\theta(t) = \theta_{\text{adia}}(t) + \varepsilon \sum a_i \sin(2\pi f_i t + \psi_i), \tag{4}$$

where $\theta_{\text{adia}}(t)$ corresponds to all phase variations with Fourier frequencies, f_{adia}, less than the Rabi frequency, and the sum is over the Fourier frequencies, f_i, in the vicinity of the Rabi frequency and higher. The ψ_i are random and uniformly distributed phases between 0 and 2π; the parameter ε represents the mean amplitude of the Fourier components near the Rabi frequency, and the a_i reflect the specific variations in Fourier amplitudes and are associated with the power spectral density of phase variations. In the present case, the Fourier frequencies associated with the adiabatic phase variations, while less than the Rabi frequency, are greater than the atom's intrinsic relaxation rate, γ. Consequently, the relative magnitudes of the key frequencies and rates in the present problem are $\gamma < 2\pi f_{\text{adia}} < \omega_1 \leq 2\pi f_i$. These relationships reflect the experimental conditions to be discussed subsequently, and allow several simplifications in the following analysis.

For realistic phase fluctuations, the adiabatic phase variations typically have larger Fourier amplitudes than the nonadiabatic variations. This prompts a perturbation approach to the analysis of Eqs. (3) in which the nonadiabatic fluctuations are treated as a perturbation to the primary response induced by the adiabatic phase variations. Each Bloch vector component is therefore written in the form

$$C(t) = C^{(0)}(t) + \varepsilon C^{(1)}(t), \tag{5}$$

where the superscripts on the Bloch-vector components indicate their order in the perturbation expansion. Inserting Eq. (5) and Eq. (4) into Eqs. (3) yields the zeroth- and first-order Bloch vector equations of motion. The zeroth-order equations take the form

$$\frac{dX^{(0)}}{dt} = -\gamma X^{(0)} + \left(\frac{d\theta_{\text{adia}}}{dt} + \Delta \right) Y^{(0)} - \omega_1 Z^{(0)}, \tag{6a}$$

$$\frac{dY^{(0)}}{dt} = -\gamma Y^{(0)} - \left(\frac{d\theta_{\text{adia}}}{dt} + \Delta \right) X^{(0)}, \tag{6b}$$

$$\frac{dZ^{(0)}}{dt} = -\gamma (Z^{(0)} - Z_0) + \omega_1 X^{(0)}, \tag{6c}$$

while the first-order equations are

$$\frac{dX^{(1)}}{dt} = -\gamma X^{(1)} + \left(\frac{d\theta_{\text{adia}}}{dt} + \Delta \right) Y^{(1)} - \omega_1 Z^{(1)} + Y^{(0)} \sum 2\pi a_i f_i \cos(2\pi f_i t + \psi_i), \tag{7a}$$

$$\frac{dY^{(1)}}{dt} = -\gamma Y^{(1)} - \left(\frac{d\theta_{\text{adia}}}{dt} + \Delta \right) X^{(1)} - X^{(0)} \sum 2\pi a_i f_i \cos(2\pi f_i t + \psi_i), \tag{7b}$$

$$\frac{dZ^{(1)}}{dt} = -\gamma Z^{(1)} + \omega_1 X^{(1)}. \tag{7c}$$

As anticipated, the first-order equations provide insight into the behavior of the atomic system at Fourier frequencies near to or greater than the Rabi frequency.

In order to simplify the first-order equations, several approximations may be made. First, since the Rabi frequency is much greater than the relaxation rate, Eq. (7c) becomes

$$\frac{dZ^{(1)}}{dt} \cong \omega_1 X^{(1)}. \tag{8}$$

Differentiation of Eq. (7a), followed by the insertion of Eqs. (8) and (7b), then results in a second-order differential equation for $X^{(1)}$,

$$\frac{d^2 X^{(1)}}{dt^2} + \gamma \frac{dX^{(1)}}{dt} + (\Delta^2 + \omega_1^2) X^{(1)} = \frac{d}{dt} \left(Y^{(0)} \sum 2\pi a_i f_i \cos(2\pi f_i + \psi_i) \right) - X^{(0)} \Delta \sum 2\pi a_i f_i \cos(2\pi f_i t + \psi_i). \tag{9}$$

[In obtaining Eq. (9) we neglected the γ term in Eq. (7b), the $\ddot{\theta}_{\rm adia}$ term in the derivative of Eq. (7a), and we assumed that $\sqrt{\Delta^2+\omega_1^2}\gg\dot{\theta}_{\rm adia}$.] Equation (9) indicates that $X^{(1)}$ responds to the PDF like a damped, driven harmonic oscillator, whose resonant frequency is the Rabi nutational frequency, $\Omega\equiv\sqrt{\Delta^2+\omega_1^2}$. Note that when the detuning is set equal to zero, the resonant frequency is just the Rabi frequency as observed in our previous investigations [2]. Since the driving frequencies in Eq. (9) are greater than or equal to the Rabi frequency, the $X^{(1)}$ response as a function of Fourier frequency will have a resonance line shape akin to that of a harmonic oscillator. In conjunction with Eq. (8), this conclusion implies that the atomic population will also display a resonant response for Fourier frequencies approximately equal to the Rabi nutational frequency. Though some distortion of the ''pure'' harmonic-oscillator resonance line shape should be expected given the integration implied by Eq. (8), qualitatively we expect this to have a small effect, as the Rabi-resonance linewidth is much narrower than the Rabi-resonance center frequency.

The strength of the Rabi resonance can be examined through the behavior of the zeroth-order Bloch-vector components, as these determine the strength of the ''force'' exciting the Rabi resonance. However, Eqs. (6), including the equations describing the motion of $\theta(t)$ and $\dot{\theta}(t)$, are nonlinear. To proceed, we therefore augment our perturbation expansion with a linearization of the zeroth-order equations in the vicinity of their equilibrium point. Within this additional, linear approximation we can investigate the dynamics of the $X^{(0)}$ and $Y^{(0)}$ components, and thereby the strength of the force exciting the Rabi resonance. (The linearization procedure is described in Ref. [4], and will not be repeated here.) The relevant results are the linearized differential equations for the zeroth-order Bloch-vector components, and their equilibrium values (i.e., $X^{\rm eq}$, $Y^{\rm eq}$, and $Z^{\rm eq}$).

Since the relaxation rate is much smaller than the Rabi-frequency and field-frequency detuning, the equilibrium values take on relatively simple forms:

$$X^{\rm eq}=-\frac{\gamma\omega_1 Z_0}{\Omega^2}, \tag{10a}$$

$$Y^{\rm eq}=\frac{\Delta\omega_1 Z_0}{\Omega^2}, \tag{10b}$$

$$Z^{\rm eq}=\frac{(\Delta^2+\gamma^2)Z_0}{\Omega^2}. \tag{10c}$$

The linearized zeroth-order differential equations are now written in terms of a primed set of variables which have been shifted from the unprimed values by the component equilibrium values (e.g., $X'\equiv X^{(0)}-X^{\rm eq}$),

$$\frac{dX'}{dt}=-\gamma X'+\Delta Y'-\omega_1 Z'+Y^{\rm eq}\frac{d\theta_{\rm adia}}{dt}, \tag{11a}$$

$$\frac{dY'}{dt}=-\gamma Y'-\Delta X'-X^{\rm eq}\frac{d\theta_{\rm adia}}{dt}, \tag{11b}$$

$$\frac{dZ'}{dt}=-\gamma Z'+\omega_1 X'. \tag{11c}$$

Differentiation of Eq. (11a) followed by substitution of Eqs. (11b) and (11c) results in the following differential equation for X' with γ small,

$$\frac{d^2X'}{dt^2}+\gamma\frac{dX'}{dt}+\Omega^2X'=\Delta X^{\rm eq}\frac{d\theta_{\rm adia}}{dt}+Y^{\rm eq}\frac{d^2\theta_{\rm adia}}{dt^2}. \tag{12}$$

Again, we obtain a damped, driven harmonic-oscillator equation with the Rabi nutational frequency as the resonance frequency. However, for this zeroth-order response all Fourier components associated with the driving terms on the right-hand side of Eq. (12) are well below the resonance frequency. Consequently, the response of X' to the PDF is like a stiff spring, simply proportional to the driving terms. Additionally, the relative magnitudes of all the parameters in the problem indicate that the term on the right-hand side of Eq. (12) containing $Y^{\rm eq}$ is dominant. The temporal behavior of X' may therefore be described approximately as

$$X'=\frac{Y^{\rm eq}}{\Omega^2}\frac{d^2\theta_{\rm adia}}{dt^2}, \tag{13}$$

leading to

$$X^{(0)}\cong\frac{\Delta\omega_1 Z_0}{\Omega^4}\frac{d^2\theta_{\rm adia}}{dt^2}-\frac{\gamma\omega_1 Z_0}{\Omega^2}. \tag{14}$$

Combining Eq. (13) with Eq. (11b) yields an expression for the zeroth-order behavior of $Y(t)$:

$$Y^{(0)}\cong\frac{\omega_1 Z_0}{\Omega^2}\left[\Delta-\frac{\Delta^2\dot{\theta}_{\rm adia}}{\Omega^2}+\gamma\theta_{\rm adia}\right]. \tag{15}$$

Equations (14) and (15) can now be substituted back into Eq. (9) to obtain an explicit expression for the force driving $X^{(1)}$. However, as the Fourier component at Ω will dominate the forcing function on the right-hand side of Eq. (9), the Bloch-vector behavior can be analyzed semiquantitatively by considering just this one Fourier component. Normalizing the differential equation so that the forcing function has units of $X^{(1)}$, Eq. (9) then becomes

$$\frac{1}{\Omega^2}\frac{d^2X^{(1)}}{dt^2}+\frac{\gamma}{\Omega^2}\frac{dX^{(1)}}{dt}+X^{(1)}=-a_\Omega Z_0A\ \sin(\Omega t+\psi_\Omega) \tag{16a}$$

with

$$A=\frac{\omega_1\Delta}{\Omega^2}\left[1-\frac{\Delta\dot{\theta}_{\rm adia}}{\Omega^2}\right]. \tag{16b}$$

(We have again ignored terms of γ and $\ddot{\theta}_{\rm adia}$.) Since the amplitude of the force term on the right-hand side of Eq. (16a) determines the magnitude of $X^{(1)}$, conditions that maximize this amplitude must also maximize the strength of the Rabi resonance as indicated by Eq. (8). The amplitude for the force term [i.e., Eq. (16b)] is therefore a measure of the Rabi resonance's strength, and this is plotted in Fig. 1 for

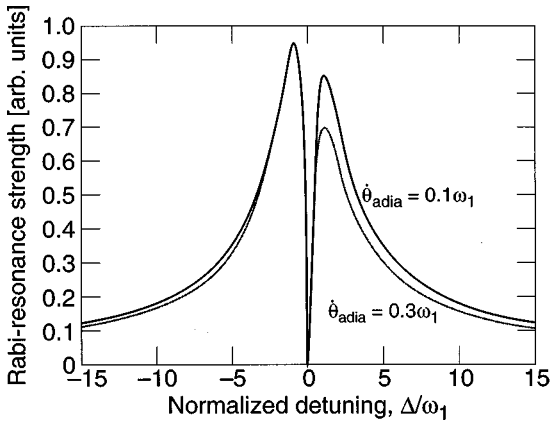

FIG. 1. Theoretical Rabi-resonance strength as a function of normalized detuning.

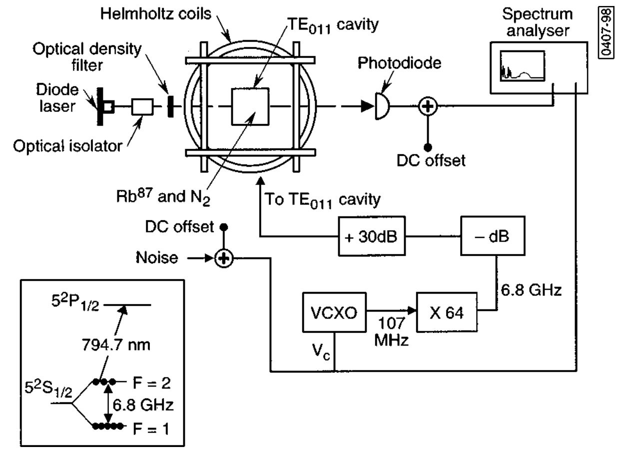

FIG. 2. Optical-pumping/magnetic-resonance experimental arrangement as described in the text. The VCXO had a bandwidth of approximately 10 kHz and a transfer function of -794 Hz/V. The bandwidth of the spectrum analyzer was 25 kHz.

two different values of $\dot{\theta}_{\mathrm{adia}}$. Note that the Rabi-resonance strength is zero for $\Delta=0$, and that it is an asymmetric function of detuning with the greater Rabi-resonance strength corresponding to $\omega_{\mathrm{field}}<\omega_{\mathrm{atom}}$. The detuning that results in the maximum Rabi-resonance strength, Δ_{max}, can be determined by finding the extremum of Eq. (16b) as a function of detuning, and this is found to occur when $|\Delta_{\mathrm{max}}|=\omega_1$.

Application of straightforward analytical techniques and judicious approximations has resulted in a simple description of the two-level atom's response to a nonresonant, phase-fluctuating field. The three principal predictions of our theoretical analysis may be briefly summarized as follows: (i) the center frequency of the Rabi resonance will equal the Rabi *nutational* frequency; (ii) the Rabi resonance's maximum amplitude will occur when the absolute value of the detuning equals the Rabi frequency, and (iii) the maximum amplitude of the Rabi resonance will be larger with the field tuned below resonance than with it tuned to frequencies above resonance. In the following section we will describe experiments that confirm these expectations.

III. EXPERIMENT

The experimental arrangement is essentially the same as that employed previously [3]. As illustrated in Fig. 2, a resonance cell containing isotopically pure ^{87}Rb and 10 torr of N_2 was placed in a microwave cavity whose TE_{011} mode was resonant with the ground-state hyperfine transition of ^{87}Rb at 6834.7 MHz. Specifically, the microwave field induced transitions between the $(F=2,m_F=0)-(F=1,m_F=0)$ ground-state Zeeman sublevels. (This is often referred to as the 0-0 ground-state hyperfine transition.) The cylindrical cavity had a radius of 2.8 cm and a length of 5 cm, and the resonance cell filled the cavity volume. The loaded cavity Q was approximately 400, though coating of the glass resonance cell by a film of alkali metal during the experiments likely reduced this considerably. Braided windings wrapped around the cavity heated the resonance cell to ~32 °C, and the entire assembly was centrally located in a set of three perpendicular Helmholtz coil pairs: two pairs zeroed out the Earth's magnetic field while the third pair (~1 G) provided a quantization axis for the atoms parallel to the microwave cavity's cylindrical axis. Light from a linearly polarized $Al_xGa_{1-x}As$ diode laser (~3 mW) was tuned to the Rb $5\,^2P_{1/2}$–$5\,^2S_{1/2}(F=2)$ transition [8], and was attenuated by a 2.7 optical density filter before passing through the resonance cell. The propagation direction of the laser was along the cavity axis; it entered the cavity through a 1.14-cm-diam port, and its transmission through the vapor was monitored with a Si photodiode.

In the absence of resonant microwaves, optical pumping reduced the density of atoms in the absorbing state [i.e., $5\,^2S_{1/2}(F=2)$], and consequently increased the amount of light transmitted through the vapor. However, when the microwave field in the cavity was resonant with the ^{87}Rb 0-0 hyperfine transition, atoms returned to the $5\,^2S_{1/2}(F=2)$ state from the $5\,^2S_{1/2}(F=1)$ state, thereby reducing the amount of transmitted light. Since the degree of optical pumping was relatively low, microwave-induced changes in the atomic population distribution were proportional to changes in the transmitted laser light. Consequently, the transmitted laser light was a measure of the atomic population's response to the fluctuating microwave field. Moreover, due to the spatial distribution of optical pumping efficiency within the resonance cell, most of the atomic signal was derived from the central portions of the cavity where the microwave magnetic-field strength (and hence the Rabi frequency) was relatively constant [9].

The microwaves were derived from a voltage-controlled-crystal oscillator (VCXO) which had a modulation bandwidth of 10 kHz [10], and the frequency of its output at ~107 MHz was multiplied up to 6.8 GHz before being amplified by a 30 dB solid-state amplifier. The microwave power entering the cavity could be controlled with variable attenuators (labeled as $-$dB in Fig. 2), and these were calibrated to microwave Rabi frequency by measuring the linewidth of the hyperfine transition in the absence of noise [11]. Extrapolating the linewidth measurements to zero microwave power indicated that the intrinsic dephasing rate in our system, γ_2, was approximately 40 Hz. The white-noise output from a commercial synthesized function generator with a 15 MHz bandwidth was added to a dc voltage in order to provide the VCXO's control voltage, V_c. The dc level of V_c fixed the detuning between the average microwave frequency

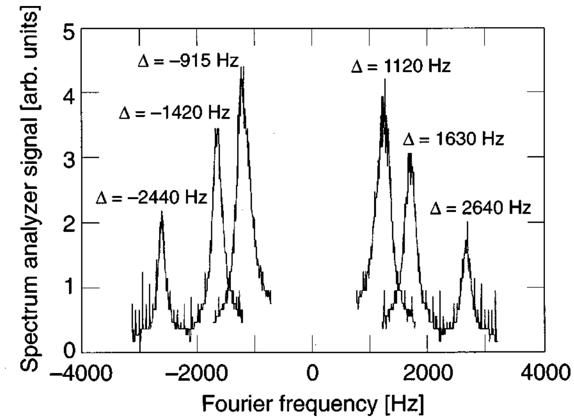

FIG. 3. Several examples of Rabi resonances as observed on the spectrum analyzer for different values of the field detuning. The Rabi frequency for this particular experiment was 950 Hz. For the purposes of this plot, negative detunings were taken to imply negative Fourier frequencies.

and the 0-0 hyperfine resonance, and the noise generator provided stochastic phase fluctuations. In contrast to our previous studies [3], there was no ''extra'' adiabatic phase variation added to the control voltage. The only adiabatic phase variation was that arising from the broadband nature of the stochastic phase fluctuations.

The noise signal and dc voltage were summed in a preamplifier with an adjustable bandwidth. The high-frequency roll-off of the preamplifier, at 6 dB/octave, was set at 1 MHz, so that the VCXO was the bandwidth-limiting element in the microwave chain and hence determined the spectral cutoff of the microwave field's frequency fluctuations. Consequently, the frequency fluctuations associated with the microwave field were white out to about 10 kHz [12]. The amplitude of the noise voltage could be adjusted in order to vary the standard deviation of the phase variations. However, for the present experiments this noise voltage was kept at a fixed value, so that the standard deviation of microwave frequency fluctuations was 250 Hz.

IV. RESULTS

The basic experimental procedure amounted to fixing a value for the Rabi frequency and detuning, and then measuring the Fourier spectrum of population variations (as monitored by the transmitted light intensity) on a spectrum analyzer. Figure 3 shows a typical set of Rabi resonances obtained in our experiment for the case $\omega_1 = 950$ Hz, and clearly demonstrates a change in the Rabi resonance's strength and center frequency with detuning. A more quantitative assessment of the Rabi-resonance condition's dependence on detuning is shown in Fig. 4, where the Rabi-resonance center frequency is plotted as a function of Rabi nutational frequency. Note that the relationship is linear, as predicted theoretically, and that this linearity is maintained for more than two orders of magnitude.

The change in strength of the Rabi resonance as a function of detuning is illustrated in Fig. 5, where (a) corresponds to $\omega_1 = 950$ Hz and (b) corresponds to $\omega_1 = 3780$ Hz. The solid line in the figure is simply an aid to guide the eye, as Eq. (16b) is only valid in a semiquantitative sense. However,

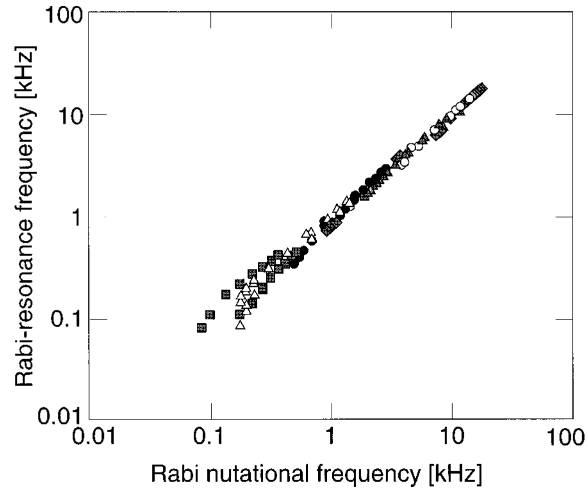

FIG. 4. Resonant frequency of the Rabi resonance versus the Rabi nutational frequency; differing symbols correspond to different values of the Rabi frequency, ω_1: for gray diamonds $\omega_1 = 7540$ Hz, for white circles $\omega_1 = 3780$ Hz, for gray triangles $\omega_1 = 1890$ Hz, for white diamonds $\omega_1 = 950$ Hz, for black circles $\omega_1 = 475$ Hz, for white triangles $\omega_1 = 170$ Hz, and for gray squares $\omega_1 = 85$ Hz. Since the amplitude of the Rabi resonance depends on the relationship between $|\Delta|$ and ω_1, different combinations of $|\Delta|$ and ω_1 were required to generate Rabi resonances with good signal-to-noise characteristics.

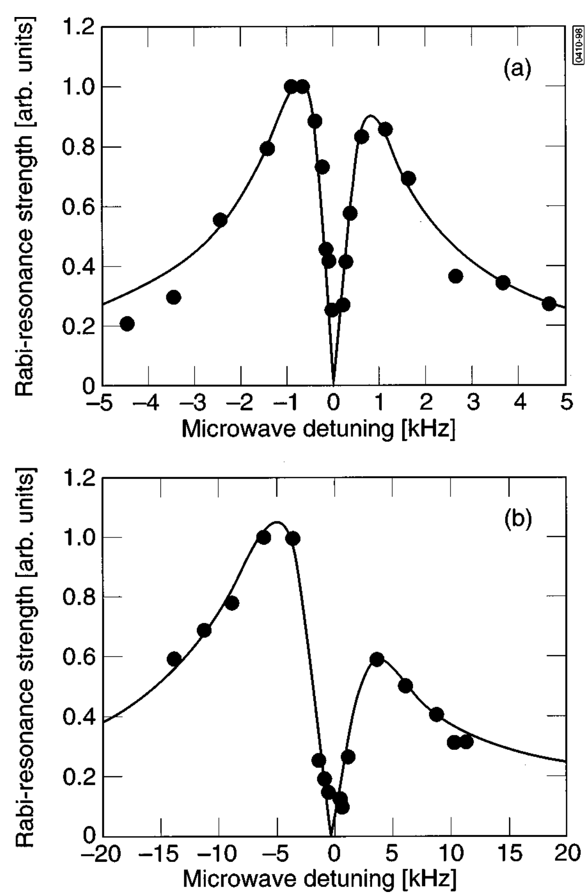

FIG. 5. Amplitude of the Rabi resonance as a function of microwave field detuning for (a) $\omega_1 = 950$ Hz and (b) $\omega_1 = 3780$ Hz.

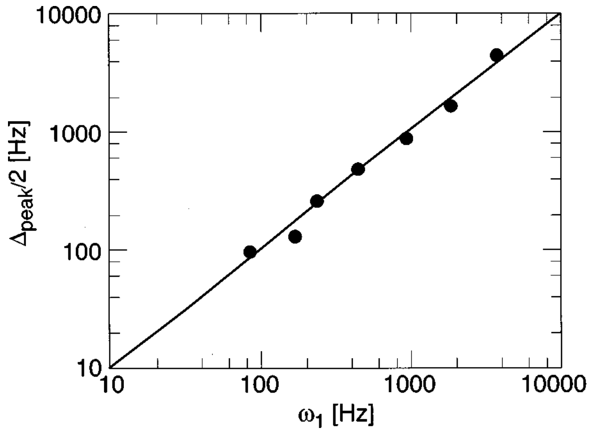

FIG. 6. Defining the separation between extrema in curves like that of Fig. 5 as Δ_{peak}, this graph plots $\Delta_{peak}/2$ vs ω_1. Basically, $\Delta_{peak}/2$ is a measure of the detuning magnitude that maximizes the strength of the Rabi resonance.

as predicted theoretically, the Rabi-resonance strength does drop dramatically for $\Delta=0$, and it is an asymmetric function of detuning with larger Rabi-resonance strengths corresponding to $\omega_{field}<\omega_{atom}$. Similar behavior was observed for all Rabi frequencies examined in our study.

In order to estimate the magnitude of detuning that maximized the Rabi-resonance strength, we used curves like those shown in Fig. 5 and measured the separation between peaks, Δ_{peak}. Half of this spacing may be taken as the detuning that maximizes the Rabi resonance, and this is shown in Fig. 6 as a function of Rabi frequency. The solid line corresponds to the theoretical prediction of $|\Delta_{max}|=\omega_1$, and is verified by the measurements for more than an order of magnitude change in the Rabi frequency.

V. SUMMARY

In the investigation discussed here, we have theoretically and experimentally expanded on our previous studies by investigating Rabi resonances excited by off-resonant stochastic fields. Our experiments are in very good agreement with theoretical expectations. Specifically we have found that (i) Rabi resonances occur at the Rabi *nutational* frequency, $\Omega=\sqrt{\Delta^2+\omega_1^2}$; (ii) the strength of a Rabi resonance is maximized when the field-atom detuning equals ω_1; and (iii) the strength of a Rabi resonance is an asymmetric function of detuning.

Though interesting in its own right, the Rabi-resonance phenomenon has application for the atomic stabilization of electromagnetic field amplitude [13]. Specifically, by phase modulating a resonant field in the manner of Cappeller and Mueller (CM) [5], it is possible to lock the Rabi frequency (and hence field strength) to the phase-modulation frequency. Since the phase-modulation frequency can be derived from an ultrastable oscillator (e.g., an atomic clock), the resulting stabilized field can exhibit extremely low intensity noise, and moreover may be precisely tuned by varying the phase-modulation frequency. With this application in mind (and to the extent that the CM manifestation of the Rabi-resonance phenomenon displays similar characteristics to ours), the present experiments show that fluctuations in the field frequency will give rise to fluctuations in the Rabi-resonance condition. In a field-strength feedback control loop these fluctuations in the Rabi-resonance condition would give rise to field strength instability. However, as the present work demonstrates, the Rabi-resonance condition is defined by the Rabi nutational frequency, and for small detunings $\Omega\cong\omega_1[1+(\Delta^2/2\omega_1^2)]$. Consequently, field frequency fluctuations would only affect field-strength stabilization using Rabi resonances in a second-order fashion.

ACKNOWLEDGMENTS

The authors would like to thank B. Jaduszliwer for several stimulating discussions regarding the experimental findings, and a critical reading of the manuscript. This work was supported under U.S. Air Force Contract No. FO4701-93-C-0094.

---

[1] Rigorously, the term PDF (i.e., phase-diffusion field) should be reserved for fields whose phase variations undergo a random walk. However, for ease of discussion we are generalizing the acronym in this paper so as to refer to any field whose phase fluctuations have a nonwhite power spectral density.

[2] R. P. Frueholz and J. C. Camparo, Phys. Rev. A **54**, 3499 (1996).

[3] J. C. Camparo, J. G. Coffer, and R. P. Frueholz, Phys. Rev. A **56**, 1007 (1997).

[4] R. P. Frueholz and J. C. Camparo, Phys. Rev. A **52**, 472 (1995).

[5] U. Cappeller and H. Mueller, Ann. Phys. (Leipzig) **42**, 250 (1985).

[6] M. H. Anderson, R. D. Jones, J. Cooper, S. J. Smith, D. S. Elliot, H. Ritsch, and P. Zoller, Phys. Rev. A **42**, 6690 (1990).

[7] It is worth mentioning that if an ensemble average were taken over Eqs. (3), the field's phase noise would give rise to an additional dephasing rate as a consequence of the fluctuation-dissipation theorem. See R. F. Fox, J. Math. Phys. **13**, 1196 (1972).

[8] J. C. Camparo, Contemp. Phys. **26**, 443 (1985); C. E. Wieman and L. Hollberg, Rev. Sci. Instrum. **62**, 1 (1991).

[9] J. C. Camparo and R. P. Frueholz, Phys. Rev. A **30**, 803 (1984).

[10] A VCXO has an output frequency that is approximately proportional to a control voltage, V_c. For a brief discussion of VCXO characteristics, see R. L. Kent, *The Voltage-Controlled Crystal Oscillator (VCXO): Its Capabilities and Limitations*, in *Proceedings of the 19th Annual Symposium on Frequency Control, Atlantic City, NJ, 1965* (National Technical Information Service, Springfield, VA, 1965), pp. 642–654.

[11] J. C. Camparo and R. P. Frueholz, Phys. Rev. A **31**, 1440 (1985); **32**, 1888 (1985).

[12] J. C. Camparo, Phys. Rev. A **54**, 410 (1996).

[13] J. C. Camparo, Phys. Rev. Lett. **80**, 222 (1998).